



Journal of Advanced Research in Applied Mechanics

Journal homepage:
https://semarakilmu.com.my/journals/index.php/appl_mech/index
ISSN: 2289-7895



Simulation of Energy Dissipation in BLDC Motor and Analysis of Speed-Acoustic Characteristics

Kardile Balasaheb Annasaheb¹ Khizar Ahmed Pathan², Abhijeet Bhikashet Auti¹, Sher Afghan Khan^{3,*}

- ¹ Department of Mechanical Engineering, KJ's Trinity College of Engineering and Research, Savitribai Phule Pune University, Maharashtra 411048, India
² Department of Mechanical Engineering, CSMSS Chh. Shahu College of Engineering, Aurangabad, Maharashtra-431002, India
³ Mechanical and Aerospace Engineering Department, Faculty of Engineering, International Islamic University, Kuala Lumpur, 53100, Malaysia

ARTICLE INFO

Article history:

Received 9 June 2023
Received in revised form 11 September 2023
Accepted 27 September 2023
Available online 5 November 2023

Keywords:

BLDC Motor; Current Frequency (Hz);
RMS Current (A); Threshold for (%r);
Noise Signal Analysis

ABSTRACT

The hybrid electric vehicle combines dual propulsion systems: one employs the traditional internal combustion engine, while the other utilizes a PMDC or BLDC motor. Generally, BLDC motors exhibit an efficiency of 85% to 90%. Conversely, the PMDC motor inherently achieves an efficiency of 88% under optimal running conditions. Moreover, improving the efficiency of both motors is impeded by their design constraints. Power losses in these motors primarily stem from factors such as heat generation in the rotor (I^2R losses), bearing friction, vibrations, and noise. This paper aims to investigate energy loss in a 4 kW BLDC motor manufactured by Bosch, attributable to speed-induced acoustic noise effects. Harmonic analysis of the phase current reveals the presence of odd-order harmonics, specifically those below the 11th order, resulting in current ripples. These dominant harmonic frequencies interact, ultimately generating noise and consuming a certain amount of power. These predominant frequencies correlate with fundamental electrical parameters: current frequency (Hz), RMS current (A), and threshold (%r), all associated with the motor's input power source. The 'K' factor, a parameter dependent on these three electrical factors, is calculated to determine harmonic stability. Variations in stable speeds (ranging from 1280 to 7500 RPM) are used to record 'K' factor readings. Based on IEEE Standard 85-1980 guidelines, motors are classified as either acceptable (OK) or not acceptable (not OK) according to their harmonic stability 'K' factor. Readings for each speed step are captured at a specific predominant frequency, facilitating subsequent comparisons. To validate the experimental findings, MATLAB/Simulink and a Fluke scope meter are employed to conduct power analyses for each motor, thus assessing energy loss attributed to noise. The waveform of the phase current proves instrumental in quantifying energy consumption in the BLDC motor. Notably, higher-frequency noise waves with shorter wavelengths entail greater energy consumption. Evaluating energy loss significantly contributes to the analysis of BLDC motor speed acoustics, serving to inform the design of energy-efficient hybrid electric vehicle models powered by BLDC motors, which are intended for customer service.

* Corresponding author.

E-mail address: sakhan@iium.edu.my

<https://doi.org/10.37934/aram.111.1.3861>

1. Introduction

Hybrid electric vehicles (HEVs) utilize both an internal combustion engine and electric motors, drawing power from energy stored in batteries [1]. The energy, whether generated by the internal combustion engine or the electric motor, is transmitted through the gear train to the wheel end. It is noteworthy that internal combustion engines typically achieve an efficiency of 60-65%, while electric motors can reach an efficiency of 85-90% [2]. This discrepancy highlights the advantages of electric motors.

HEV models often employ BLDC (Brushless DC) motors due to their superior efficiencies [2, 3]. With no use of brushes, the BLDC motor offers numerous advantages, including a high torque-to-inertia ratio, high speed, power density, and lower cost compared to conventional brushed-type motors [4]. This research has been conducted to analyze the contribution of noise to energy dissipation by comparing simulation results with experimental observations [5]. This study can be further enhanced to test the EMS performance of motors [4, 5]. It has already been proven that electromagnetic forces and structural modes are not the major noise sources, as the noise characteristics are not closely related to the motor RPM [6]. Acoustic modal analysis has revealed that the acoustic mode of the internal airspace of the motor is the primary source of the noise [7]. As stated by Sir Nikola Tesla, "If you wish to understand the universe, think in terms of energy, frequency, and vibration" [8]. Mechanical impedance occurs when a structure resists motion subjected to a harmonic force with acting velocities [8, 9]. The ratio of the applied force at a point on the structure to the resulting velocity at that point is the key input for speed-acoustic analysis. The type of torque generated by the BLDC motor initiates the sound waves. The mathematical relationship between BLDCM torque, air gap flux, and armature current is shown in Eq. (1) [9]:

$$T = C_T \cdot \Phi \cdot I \quad (1)$$

where T = Torque, C_T = Torque Coefficient, Φ = Air Gap Flux, I = Armature Current.

In both scenarios, energy flows through transmission lines, overcoming frictional losses, heat dissipation, noise, and vibration [10]. In this context, the noise produced by the BLDC motor is quantified using electrical parameters such as current frequency, RMS current, and threshold frequency, which are measured using an experimental setup across equally spaced speed ranges [11]. The current frequency, measured in hertz (Hz), refers to the number of current cycles per second in an alternating current sine wave [11, 12]. The RMS current value of the sine current wave is determined by the area covered in a half-cycle, which typically exceeds the average current value [13]. The threshold frequency (ν) represents the motor's minimum operating frequency at which it starts to bear a loading torque [14]. These electrical parameters are measured before reaching the resonant frequencies, where the mechanical impedance remains lower. At these frequencies, less force is required to induce movement in the structure [14, 15].

The designated armature current frequency is denoted as f_I and is related to the number of poles. The mathematical relationship between motor speed, frequency, and current is illustrated in Eq. (2) [15].

$$\eta = \frac{60f_I}{p} \quad (2)$$

where the k-factor also referred to as the stability factor, determines the total harmonic current that a motor can endure.

Drawing from ANSI/IEEE C57, while staying within the specified current threshold limits, the K-Factor in the realm of electrical parameters is quantified for non-linear loads [16]. The K-Factor represents the ratio between supplementary losses arising from harmonics and the eddy current at a frequency of 60Hz [17]. Measurement of the K-Factor involves the utilization of the Fluke 125 industrial oscilloscope meter to detect audible noise (vibration waves) in motors (with recognition of Fluke 125B+) [17, 18]. Readings are obtained from the BLDC motor test bench, with revolutions reaching a maximum of 7500 RPM under no-load conditions at free speed [19]. Figure 1 illustrates a comprehensive graph depicting the relationship between torque, power, speed, current, and efficiency [19, 20].

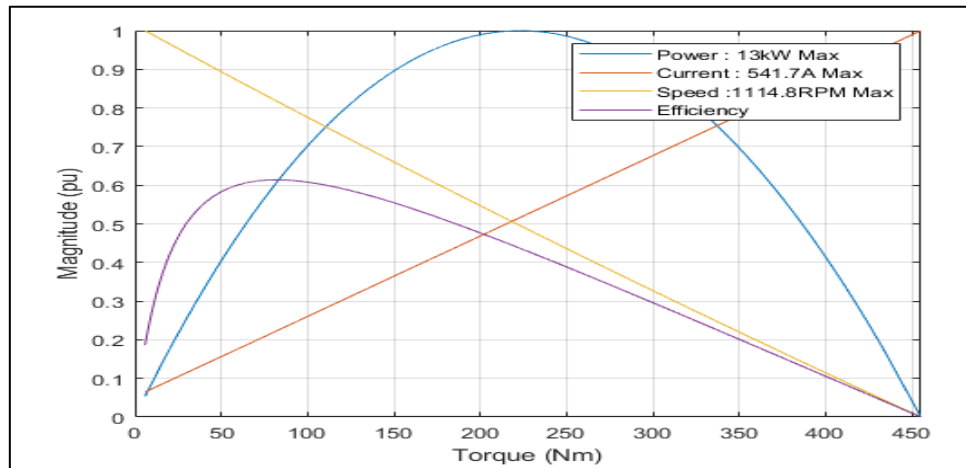


Fig. 1. BLDCM/PLDCM Connected to a Laptop-Based MATLAB/Simulink Model

The acquired reading data for these parameters is tabulated along with the K factor to classify noisy and okay motors, based on the ISO 7919-2:2001 guidelines [21]. For okay motors, experimental readings are manipulated in MATLAB/Simulink to prepare the motor control algorithm [22]. All of the following parameters: current frequency (Hz), RMS current (A), and threshold (%) are compared on the MATLAB/Simulink platform for signal analysis [23]. MATLAB/Simulink is employed to simulate and evaluate the overall energy contribution of noise in energy dissipation in BLDC motors marked as okay [24-26]. Readings are typically collected at the stable speed state of the BLDC motor, where the noise-embedded frequency is higher [27]. The study of energy consumption is conducted to test the proposed hypotheses through this simulation analysis [28].

Zi-Qiang Zhu (1991) estimated, using Finite Element Method (FEM) and Fourier analysis, that the acoustic noise in the Brushless DC (BLDC) motor is generated from a radial field of the internal rotor [1]. Yang Quan Chen *et al.*, (2009) simulated a numerical fractional-order motor controller for instant start and stop [2]. Jose Carlos Gamazo *et al.*, (2010) improved the functional reliability of shaft encoders, resolvers, or Hall-effect probes for higher performance [3]. Shalabh Rakesh Bhatnagar (SRB) (2012) used piezoelectric material to convert sound energy into electricity [4]. Madhurima Chattopadhyaya *et al.*, (2012) derived mathematical expressions based on motor working principles to achieve precise motor tracking torque [5].

Dong Ming Zhang *et al.*, (2014) proposed a Phase-Locked Loop (PLL) solution for noise rejection through PLL-based linear filtration [6]. Hong Joo Lee *et al.*, (2015) revealed that the major noise source is the internal air space among the poles [7]. Li Yaohua *et al.*, (2015) testified to the effectiveness of the Hybrid Electric Vehicle (HEV) individual element Simulation [8]. Rajamani Senthil Kumar *et al.*, (2015) introduced a Particle Swarm Optimization (PSO) based Fractional-Order

Proportional-Integral (FOPI) controller for excellent time-domain performance, disturbance rejection, and robustness [9]. Guoyuan Qi (2017) identified energy dissipation sources and critical parameters for energy consumption [10]. Kun Xia *et al.*, (2017) studied Electromagnetic Torque Ripple-induced acoustic noise in BLDCM [11]. Dr. S. K. Mahobia (2017) experimented with voltage-based RPM control using a speed controller [12]. R. M. Pindoriya *et al.*, (2018) introduced methods for suppressing acoustic noise in BLDC motor drives [13]. Sathish Kumar *et al.*, (2018) controlled the speed of the DC motor by varying stator winding voltage [14]. Durgesh Sarankar *et al.*, (2018) developed a fifth-order three-switch converter for boosting operation [15]. Rabah Djekidel *et al.*, (2018) introduced Simplex Simulated Annealing (SIMPASA) to provide optimal position and number of fictitious charges for accurate calculation of Core Saturation Magnetization (CSM) for power consumption in BLDCM [16]. Saurav Prajapati *et al.*, (2018) compared the FOPI controller with the integer-order Proportional-Integral (IOPI) controller for improved performance [17]. Jongkyong Lee *et al.*, (2018) proposed an Electromagnetic Compatibility (EMC) model of low voltage BLDCM for analyzing frequency response and minimizing noise [18]. Yogesh Singh (2019) analyzed electromagnetic forces causing vibration and acoustic noise in BLDCM [19]. Fredy E. Hoyos *et al.*, (2019) observed smaller load resistance values and errors in estimating power losses [20]. Abrar Ahmed *et al.*, (2019) developed a simulation model to compare BLDCM performance against conventional engines [21]. Yongchao Wang *et al.*, (2020) simulated noise optimization methods for electromagnetic Noise, Vibration, and Harshness (NVH) verification [22]. Ishita Gupta (2020) analyzed BLDCM for enhanced performance using simulations [23]. Allan G. Soriano-Sánchez *et al.*, (2020) proposed a non-integer Proportional-Integral-Derivative (PID) controller for regulating voltage in a DC-DC Buck converter [24]. Virlan Bogdan *et al.*, (2021) developed special software for increasing motor speed at low resistance torque, employing 24 stator slots and 22 rotor permanent magnets [25]. Zhaoyang Fu *et al.*, (2021) investigated fault signal diagnosis methods for dual redundancy BLDCM winding fault analysis [26]. Chaithanya D *et al.*, (2021) demonstrated the conversion of sound, a non-continuous form of energy, into electrical energy using piezoelectric material [26]. Mervin A. Boco (2022) converted sound energy into clean and renewable electricity [27]. Lucy Maybury (2022) investigated mathematical models for improving BLDCM efficiency [28].

Continuous operations of the BLDC motor involve loading up to the rated torque, starting from a standstill speed and accelerating. Extra torque is required to overcome load and rotor inertia. The motor delivers higher torque up to the maximum peak point if it follows the speed-torque curve, as shown in Figure 1. As speed increases to the maximum motor torque value, the torque range is consistently maintained up to the rated speed. Beyond the rated speed, the motor's torque starts to decrease. Noise performance of the motor is better with half load than with full load, where energy dissipation is also lower.

The problem with previous research on BLDC motor noise frequency is identified. Users have limited ability to change motor parameters, unlike state-space models of BLDC motors. Flexibility in speed and torque control parameters in BLDC motors is restricted. Under motor overload conditions, parameters like the speed-torque plot can enter the negative region due to drastic changes in motor characteristics. Large oscillations occur under overload conditions, leading to jerky motor operation. Various mitigation techniques are employed to enhance BLDC motor efficiency and passenger acoustic comfort. This study can be extended to identify different nonlinear variables related to the motor and its control.

The research's objective is to minimize energy dissipation in a BLDC motor. Energy dissipation occurs due to noise, vibration, heating, harmonics, etc. This study demonstrates the conversion of sound energy into electrical signals in BLDC/PMDC motors. It evaluates energy consumption by the motor up to full RPM under no-load conditions. Furthermore, the study highlights noise energy's

contribution to the overall efficiency of the BLDC motor. The research optimizes motor control parameters in coordination with noise frequency tests to develop an energy-saving Hybrid Electric Vehicle (HEV) model. Power electronics components for noise generation are studied using hardware-in-the-loop (HIL) testing.

2. Methodology

The process of identifying noise sources in a BLDC motor considers both electromagnetic forces and structural acoustic modes. A thorough analysis of the acoustic noise in BLDC motor drives will be conducted following the ISO standards. The steps for conducting the simulation experiment on the BLDC motor are depicted in Figure 2.

It has been analyzed the BLDC motor product to identify the parameters contributing to noise. We established a methodology for conducting experiments on it. Additionally, reviewed the literature to ascertain that harmonics are critical parameters responsible for noise generation in any signal waveform. These harmonics are typically present in phase current and voltage signals. The modulation of the waveform's width of these current and voltage signals would reveal the harmonic contents within them.

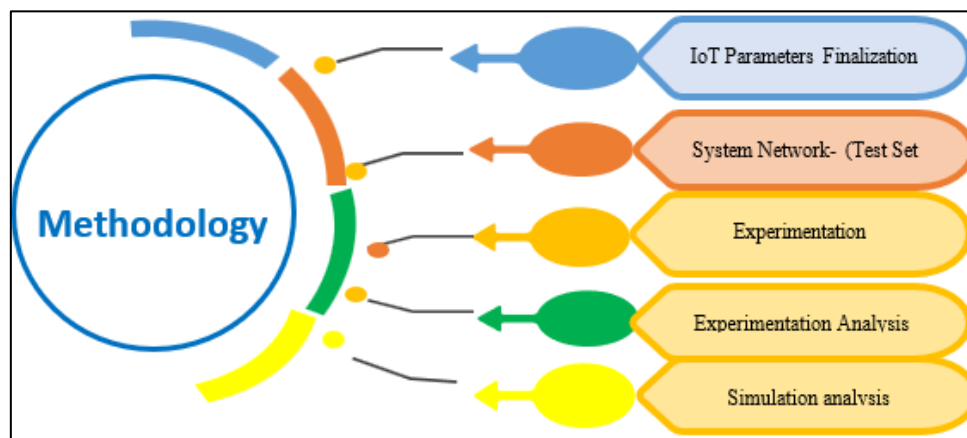


Fig. 2. Methodology for Variable Measurement

- i. The frequency represents the rate at which the current changes direction per second. Thirty motors that were procured for production underwent motor testing.
- ii. The tests were conducted at four speeds: 10 km/h, 15 km/h, 31 km/h, and 63 km/h.
- iii. During the testing phase, significant amplitude peaks were identified from the results of each test for every speed. The corresponding frequency values at these significant peaks were recorded, along with the average frequency range for each peak.
- iv. This frequency range establishes a provisional measurement zone against which the amplitude can be assessed.
- v. A datasheet was compiled, encompassing all these amplitude values, their corresponding frequencies, and the range of limits for the four speeds, encompassing the 30 distinct motors.
- vi. Using this datasheet, the average amplitude and maximum amplitude for each peak were calculated after excluding motors with the highest and lowest relative amplitudes.
- vii. With these frequency ranges derived from the pool of 30 motors, it is possible to examine the NOT OK motors to identify any notable discrepancies in the amplitude peaks within these frequency ranges.

2.1 Technical Specifications of a 5 HP BLDC Motor with a Shaft Diameter of 14.90 mm

The BLDC motor of the electric vehicle CTL H105A is utilized for the experimentation. The specifications of the BLDC motor for the electric vehicle CTL H105A are as follows:

Table 1

Technical Specification of BLDC Motor (Source: Bosch Technical Data Sheet for Customized BLDC Motor)

Description	Value
Motor Type	BSD 48V 4kW
E-Vehicle Type	48V 30A PMSM two-wheeled type
Voltage	50.4 ±0.5V
Battery DC Current Limit	≤ 90A
Phase current Limit	≤ 200A (Peak Value)
No Load DC Current	≤ 10A@7500 rpm
No Load RPM	7500 rpm@50.4 V DC
Rated Operating Point	7.4 Nm@5000 ±3% rpm, 3.8 kW
Rated Efficiency	> 85.8%@7.4 Nm, 5000rpm
Max. Torque	16± 0.5 Nm (From 0 to 2000 rpm) for 6 Min. w/o external cooling
Pick the Power of the Motor	3.4 kW (16Nm@2200rpm) at 120A Phase current (rms) for 6 Min.
Mechanical Speed Limit	9000 rpm for 2 min.
Phase Sequence	U: Yellow, V: Green, W: Blue
Poles	Stator: 12 Poles: Rotor: 10 poles

2.2 Finalizing IoT Parameters for BLDC Motor Experimentation

The BLDC motor model is prepared in MATLAB/Simulink in a manner analogous to that of a three-phase synchronous machine. As the rotor is equipped with a permanent magnet, its dynamic characteristics are depicted differently. The flux linkage from the rotor depends on the properties of the mounted permanent magnet. Similar to a typical three-phase motor, the BLDC motor's structure is energized by a three-phase input voltage source, where K_E represents the back emf constant, and ω signifies the angular speed of the rotor.

The permanent magnet also influences the produced torques due to the trapezoidal flux linkage resulting from its characteristics. K_T stands for the torque constant. The mathematical relationship between the resultant torque and the load torque, involving motor inertia (J), angular acceleration (ω), damping constant, and angular velocity as shown in Eq. (3), is corroborated by Newton's second law of motion.

$$T_{E(t)} - T_{L(t)} = J \frac{d\omega(t)}{dt} + B * \omega(t) \quad (3)$$

where T_E , Engine Torque; T_L , Load Torque; are in N-m; J , Rotor Inertia in $[kgm^2]$; and $d/dt \omega(t)$, Acceleration; B , Damping Constant

The analogs of electrical parameters of the BLDC motor, such as current frequency (Hz), RMS current (A), and Threshold (%r), are measured on the test bench to evaluate the harmonic stability factor 'K' for various stable speeds. The energy of the sound wave is calculated using the following Eq. (4).

$$E = \frac{1}{4} (A^2 \omega^2 \lambda) \quad (4)$$

where A represents the amplitude of the wave (in meters), ω denotes the angular frequency of the wave oscillator (in hertz), and λ stands for the wavelength (in meters)

2.3 Test Setup for Experimentation

Figure 3 below depicts the models of a BLDC (Brushless DC) motor and a PMDC (Permanent Magnet DC) motor, each accompanied by an electronic speed controller. These motor models are interconnected with a MATLAB/Simulink simulation through an Arduino unit, which is energized by a solar photocell. This configuration facilitates the supply of motor inputs for the simulation.

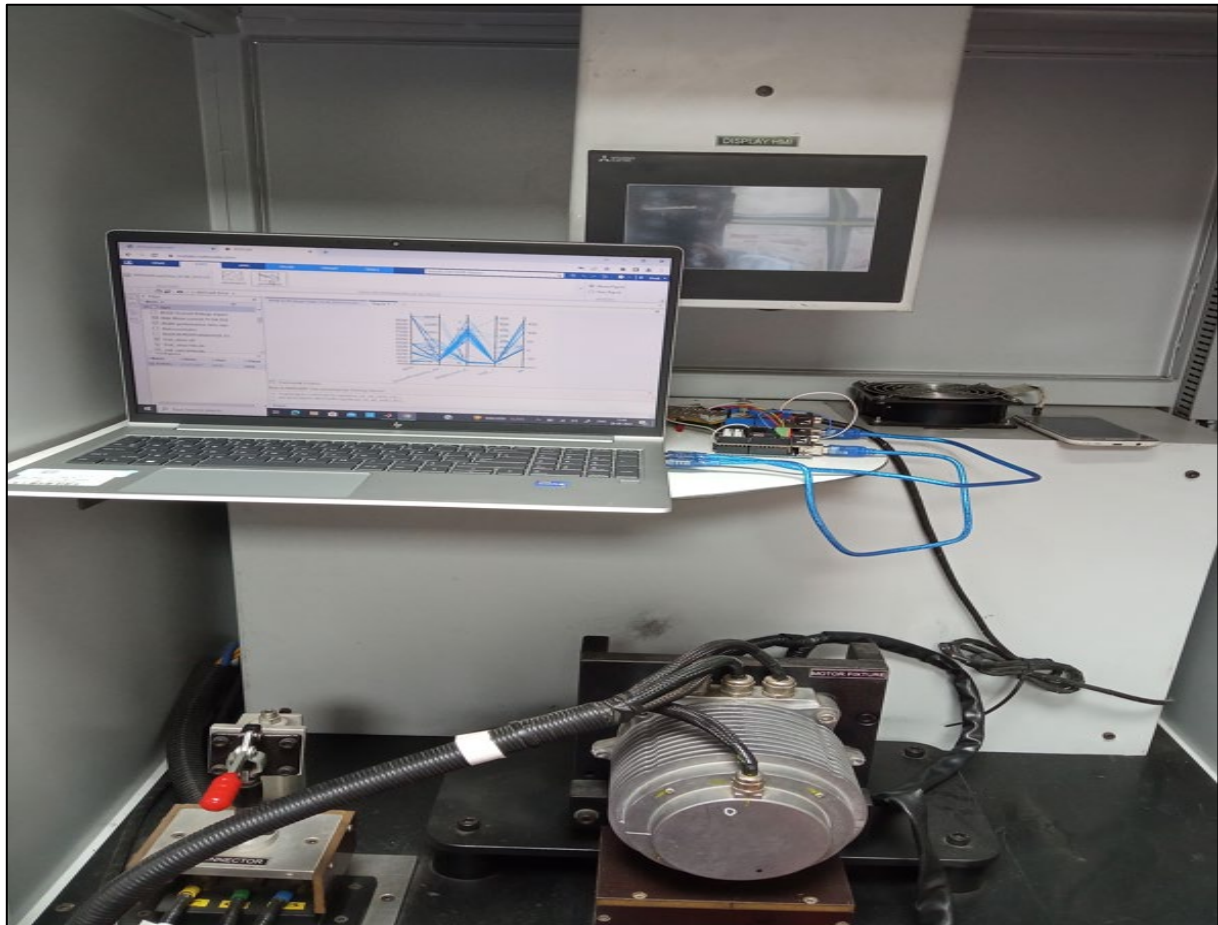


Fig. 3. BLDCM/PLDCM Connected to a Laptop-Based MATLAB/Simulink Model

The experimental setup for the BLDC motor test bench, including its components such as the motor control unit, battery management unit with battery, and Fluke device, performs a 125 B power analysis, as illustrated in Figure 4a, 4b, 4c, and 4d, respectively.



(a) Motor Test bench set up



(b) Motor Controller, Motor, BMS module, Battery



(c) Digital Oscilloscope Meter



(d) Digital L-C-R Meter

Fig. 4. Test Bench Setup of BLDCM/PLDCM with Its Components and Instruments: A Technical and Scientific Perspective

2.4 BLDC Motor Simulink Model

The block diagram for BLDC motor control is constructed within the Simulink model, incorporating the necessary control circuit elements. A MATLAB/Simulink model of a BLDC motor is created using mathematical equations for simulation purposes, as depicted in Figure 5. This paper presents a simulation-based investigation of a brushless direct current (BLDC) motor under varying no-load operating conditions. The analysis encompasses the assessment of the impact of alterations in operating conditions on the acoustic noise and vibration generated by this drive model.

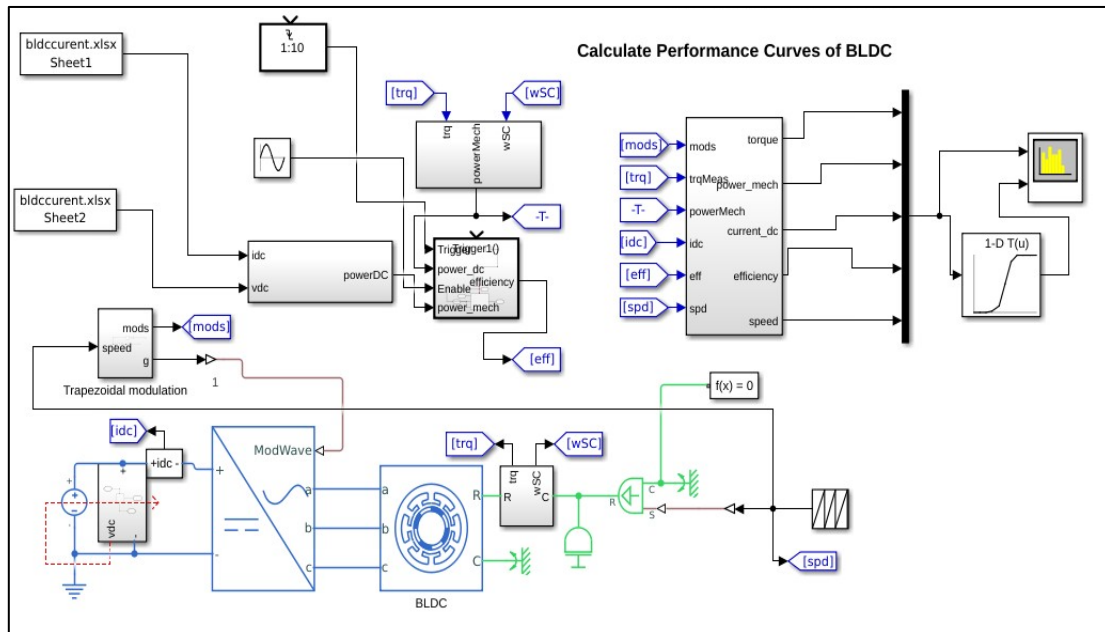


Fig. 5. Open-loop control of a 4 kW BLDC motor (utilizing 6-Step Commutation) using MATLAB/Simulink

The torque and power curve characteristic of a BLDC motor is typically shown as a function of motor rotational speed, as depicted in Figure 1. However, the motor-induced torque is not only dependent on the stall torque but also on the speed. Additionally, the rotational speed under no-load conditions remains constant [20].

3. Simulation Analysis

The data for the threshold frequency are collected using a FLUKE-125B power analyzer to analyze the phase current at various harmonic states and stable speeds. Total Harmonic Distortion (THD) refers to the arithmetic deviation in voltage or current waveforms from their ideal sinusoidal shapes. THD quantifies the undesired harmonics in the voltage or current waveforms through fast Fourier analysis. This analysis is critical for maintaining and enhancing the stability of the power supply system. Harmonic stability determines the frequency of a generated sound wave. Harmonic distortion is a term that relates threshold (%r) to stable speed, used to identify whether motors are in an acceptable condition (OK) or not (NOT OK). The threshold frequency is the minimum frequency of incident light at which the emission of electrons begins.

The frequency-amplitude spectrogram of the BLDC motor is depicted in Figure 6(a) and 6(b). These figures illustrate that at specific frequencies, higher amplitudes are observed. This phenomenon is accompanied by broader wavelengths, indicating significantly lower energy dissipation compared to the PMDC motor. This distinction is highlighted by the acoustic noise characteristics.

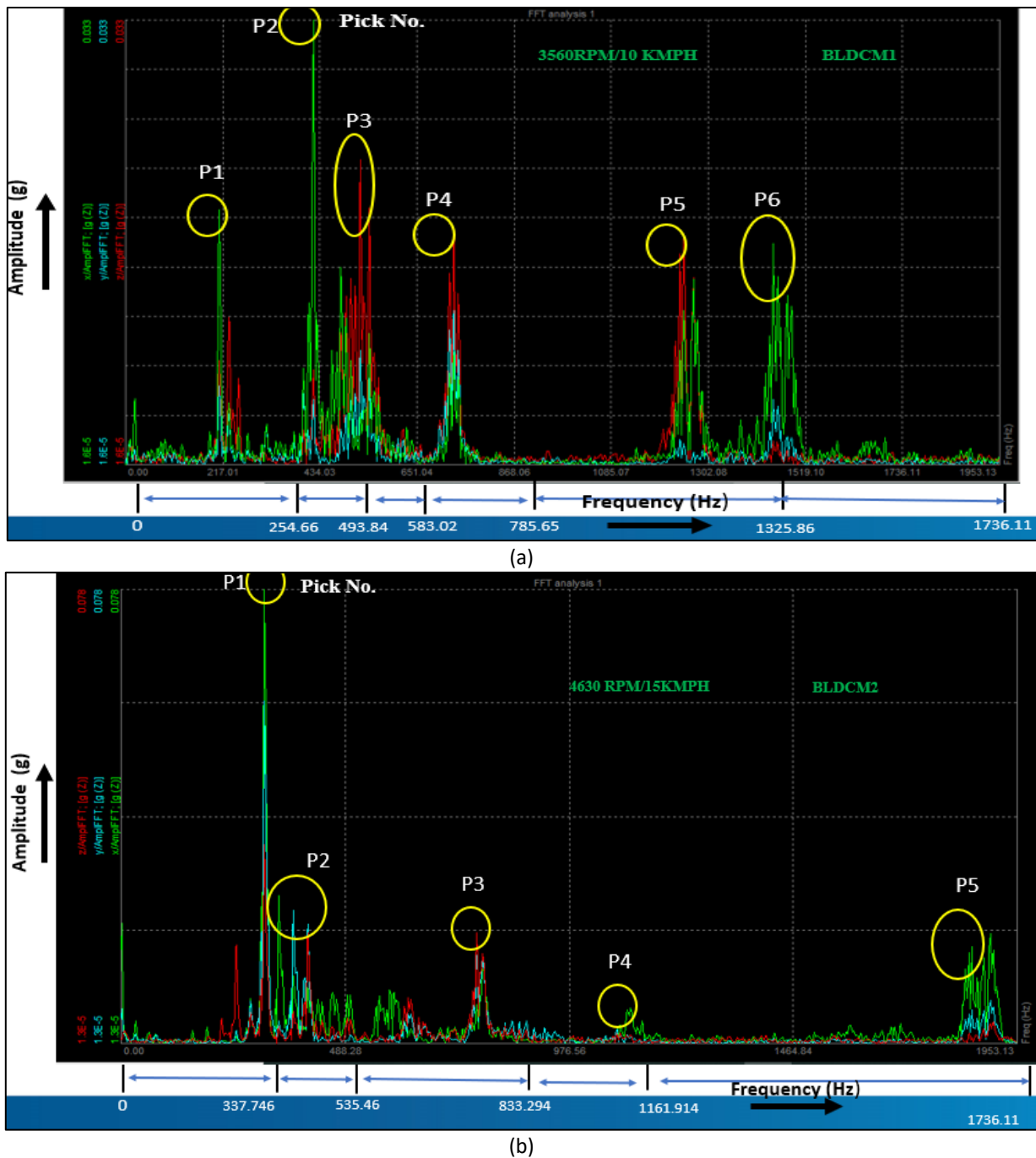
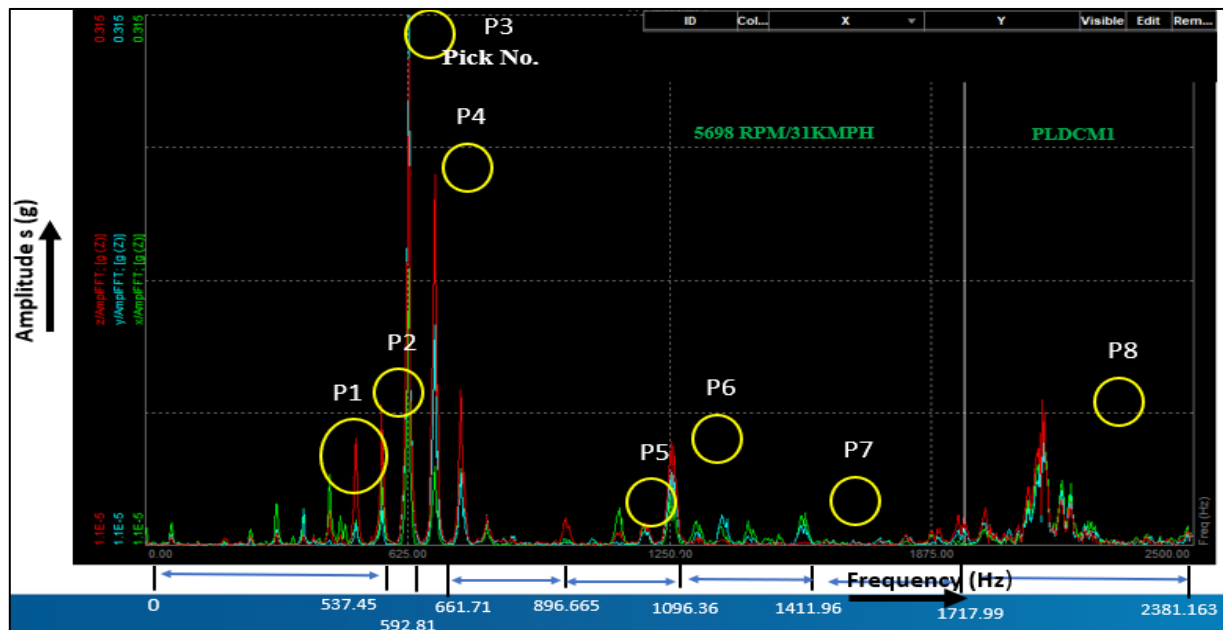


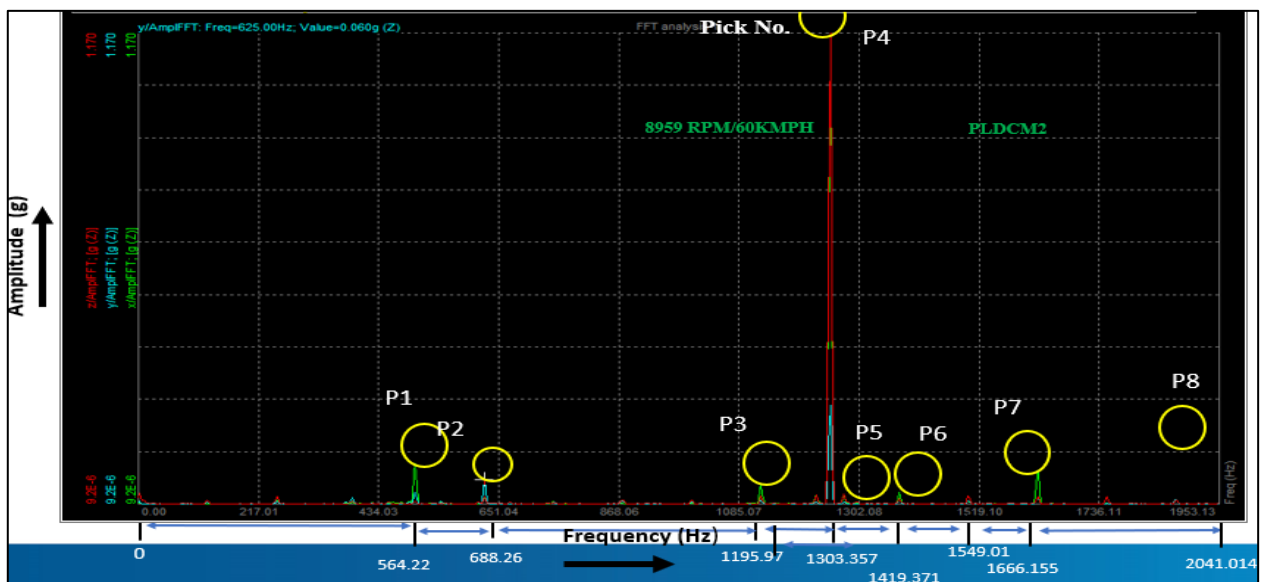
Fig. 6. Frequency-Amplitude Spectrogram of BLDC (a) Motor 1 (b) Motor 2

The frequency-amplitude spectrogram of the PMDC motor is depicted in Figure 7(a). This illustration demonstrates that at lower frequencies, a greater amplitude is observed, accompanied by a shorter wavelength. These observations indicate enhanced energy dissipation through the acoustic noise characteristics.

The frequency-amplitude spectrogram of the PMDC motor is depicted in Figure 7(b). It shows that at a specific frequency, the amplitude is generally shorter, except for point P4, which exhibits a shorter wavelength and lower energy dissipation compared to PMDC motor 1, as indicated by its acoustic noise characteristics.



(a)



(b)

Fig. 7. Frequency-Amplitude Spectrogram of PMDC (a) Motor 1 (b) Motor 2

3.1 3D Graphical Analysis

Graphical 3D surface plots are used to visually compare the expressed readings exclusively at a specific predominant frequency for each speed increment, with a) Mt. Bruno Elevation, and b) Volcano Surface Plot, facilitating in-depth analysis as depicted in Figure 8(a) and 8(b).

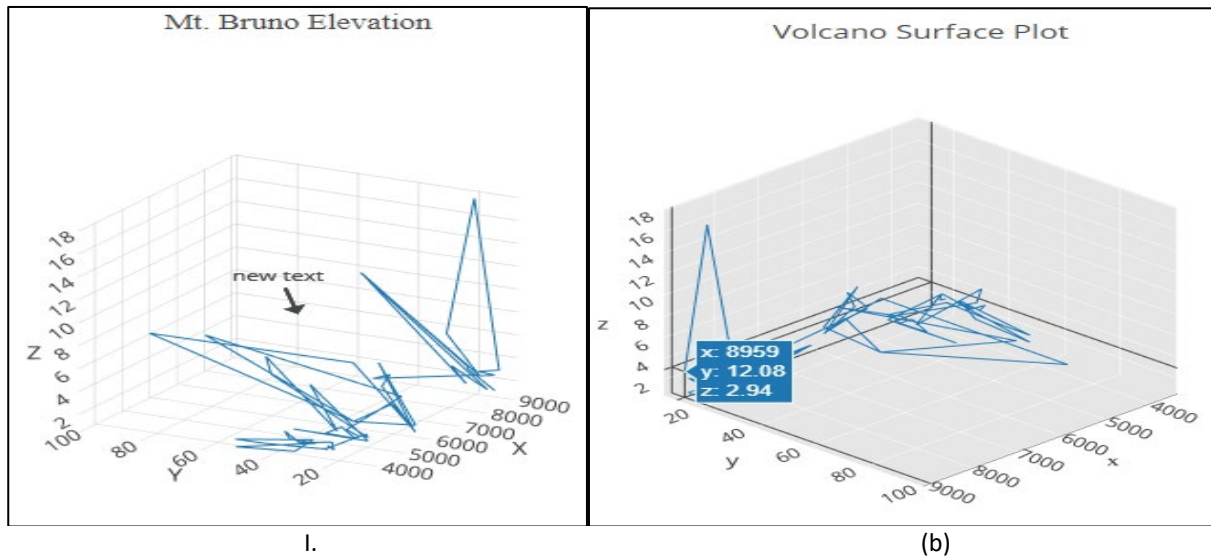


Fig. 8. Effects of RPM Input on Threshold and Harmonic Distortion Factor: A Study using the FLUKE-125B Power Analyzer with (a) Mt. Bruno Elevation and (b) Volcano Surface Plot

It appears that the Harmonic Stability K factor (KF) is calculated as follows:

$$KF = \frac{RMS\ current\ (A)}{RPM \times Current\ Frequency\ (Hz) \times \frac{THD(\%r)}{100}} \quad (5)$$

where KF is the Harmonic Stability factor, RMS is the Root Mean Square, A represents current in Amperes, RPM stands for Revolutions Per Minute of the Motor, and THD denotes Total Harmonic Distortion.

MATLAB/Simulink should be used to plot the general scale for RMS current (in amperes), current frequency (in hertz), and threshold (in the percentage of r) for BLDC motor 1, covering the range from 1280 to 7500 RPM, as illustrated in Figure 9.

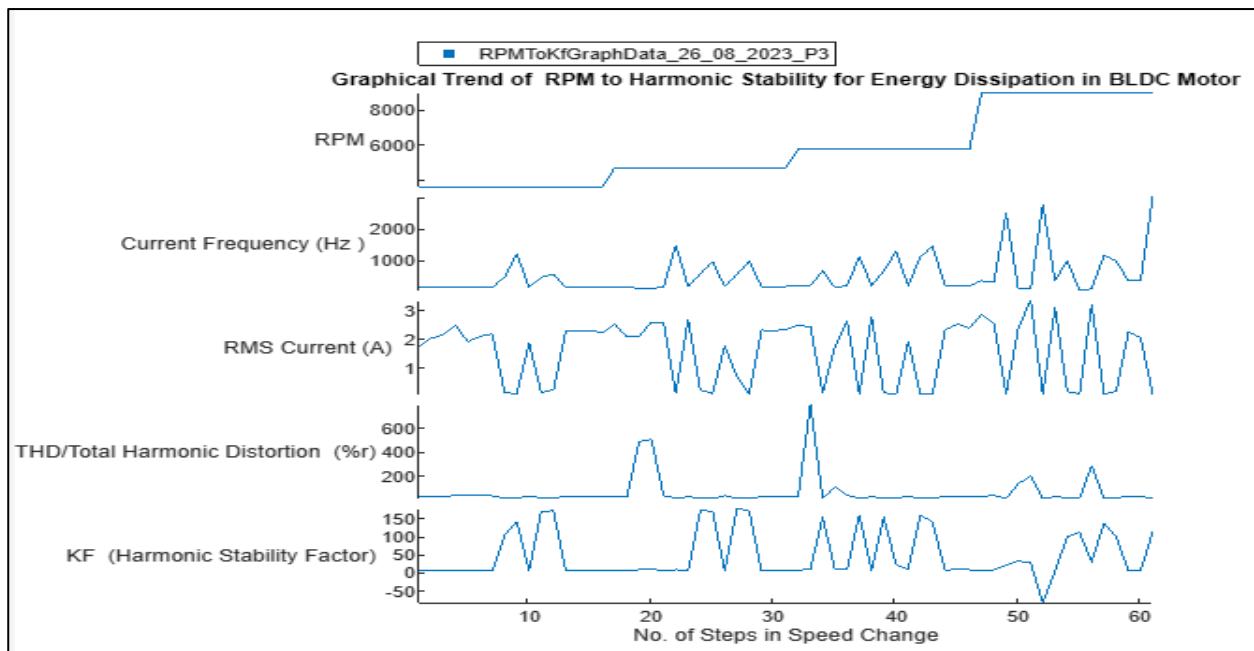


Fig. 9. The graphical trends of RMS current (A), current frequency (Hz), and Threshold (%r) for BLDCM are presented (Stacked Plot)

The graph illustrates the inverse relationship between RPM and harmonic stability in the energy dissipation of a BLDC motor. The diminishing harmonic stability with increasing RPM points to reduced energy dissipation efficiency, attributed to heightened inductance in the motor windings at higher RPMs causing current ripples and subsequent losses. The graph shown in Figure 10, also indicates an optimal RPM for maximum energy dissipation efficiency, subject to motor design and load specifics. While a valuable tool for BLDC motor engineers, it's important to note the graph's simplification, its dependency on motor characteristics and load, and its representation of a singular operating scenario rather than a comprehensive performance overview.

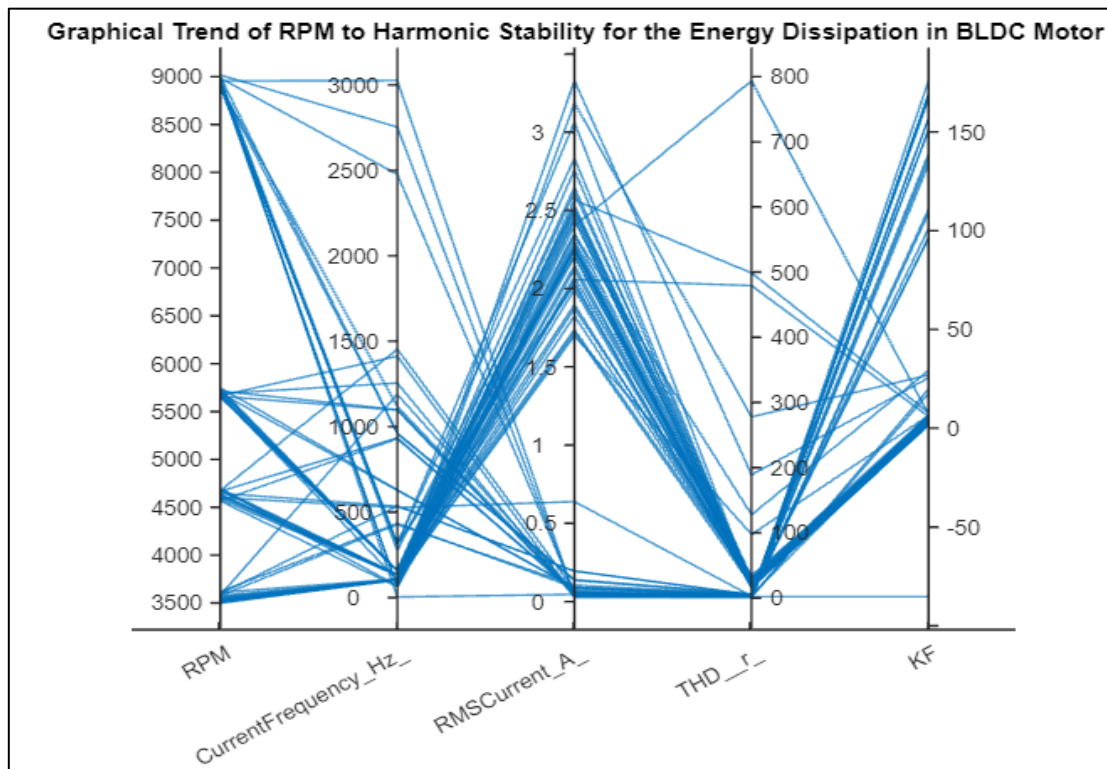


Fig. 10. The graphical trends of RMS current (A), current frequency (Hz), and Threshold (%) for BLDCM are presented (Stacked Plot)

The MATLAB/Simulink graphical plot in a logarithmic scale is used for displaying RMS current (in Amperes), current frequency (in Hertz), and threshold (in percentage of rated current) for PMDC motor 1. The plot covers the RPM range from 1280 to 7500 RPM, as depicted in Figure 11 of the reference.

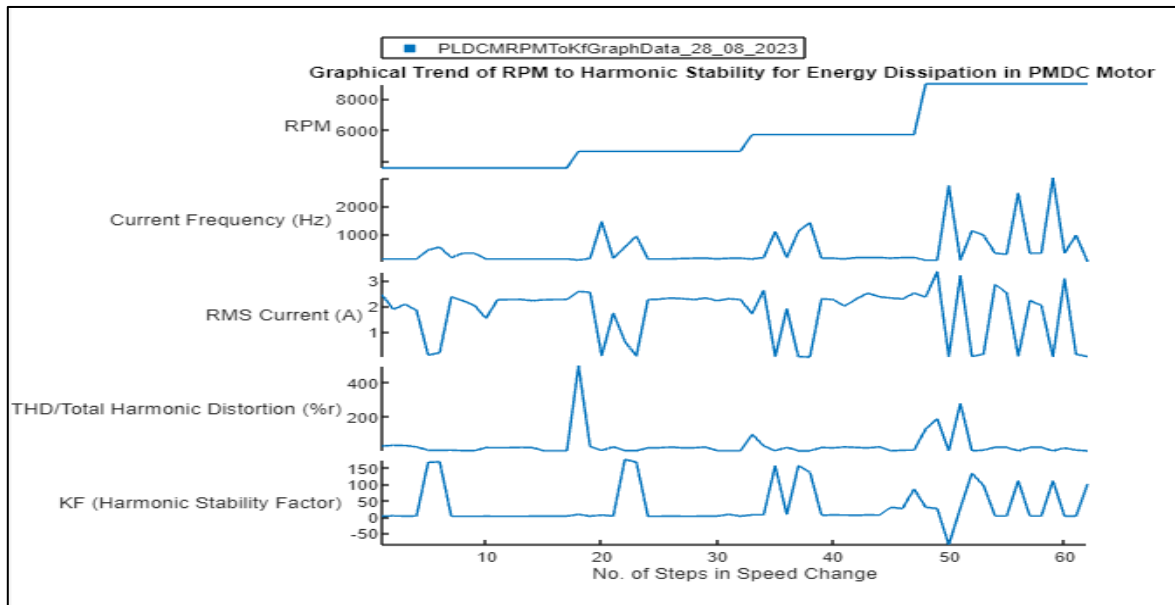


Fig. 11. Graphical logarithmic trends of RMS current (A), current frequency (Hz), and Threshold (%r) for PMDCM (Stacked Plot)

The provided graph in Figure 12 illustrates the correlation between RPM and harmonic stability in the energy dissipation of a BLDC motor. With RPM on the x-axis and harmonic stability on the y-axis, the declining trend of harmonic stability as RPM increases suggests reduced energy dissipation efficiency at higher rotational speeds. This phenomenon arises due to heightened motor winding inductance at elevated RPMs, resulting in more pronounced current ripple and associated losses that compromise efficiency. Notably, the graph highlights an optimal RPM point characterized by peak harmonic stability, indicating the motor's most efficient energy dissipation state. The determination of this optimum RPM hinges on motor design specifics and operational load considerations. While a valuable tool for BLDC motor design and troubleshooting, the graph's simplified nature underscores that the genuine RPM-harmonic stability relationship can be intricate and nonlinear.

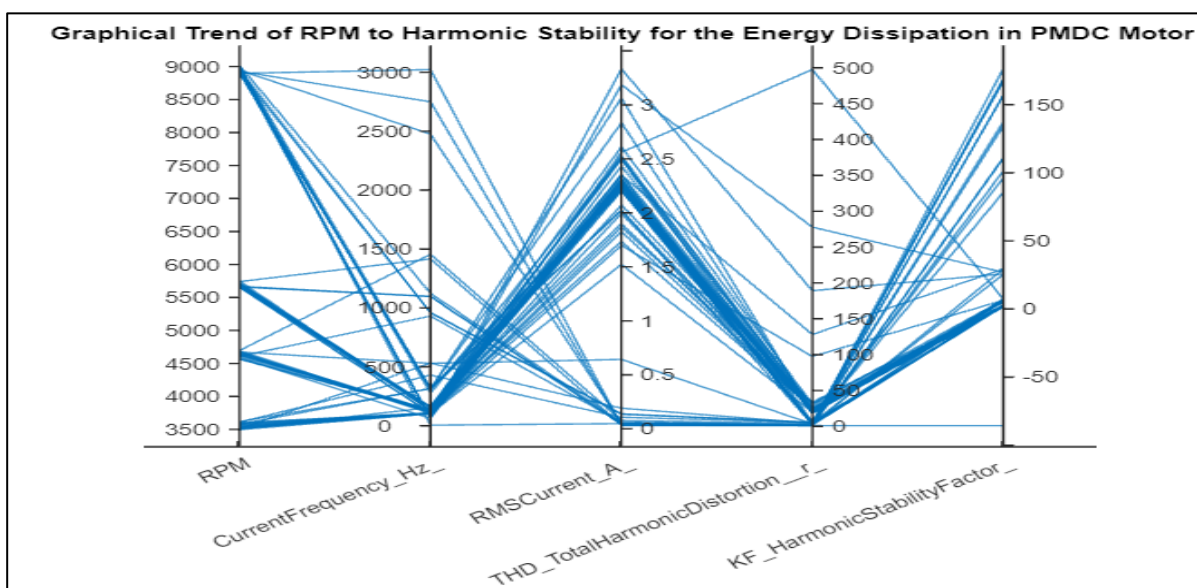


Fig. 12. Graphical logarithmic trends of RMS current (A), current frequency (Hz), and Threshold (%r) for PMDCM (Parallel Plot)

3.2 Simulation Results

MATLAB/Simulink simulations were conducted to generate spectrograms from the oscilloscope data, investigating the influence of RMS current (in μA), current frequency (in Hz), and threshold (expressed as %R), on harmonic distortion and the overall threshold for a BLDC motor operating in the range of 1280 to 7500 RPM, as depicted in Figure 13.

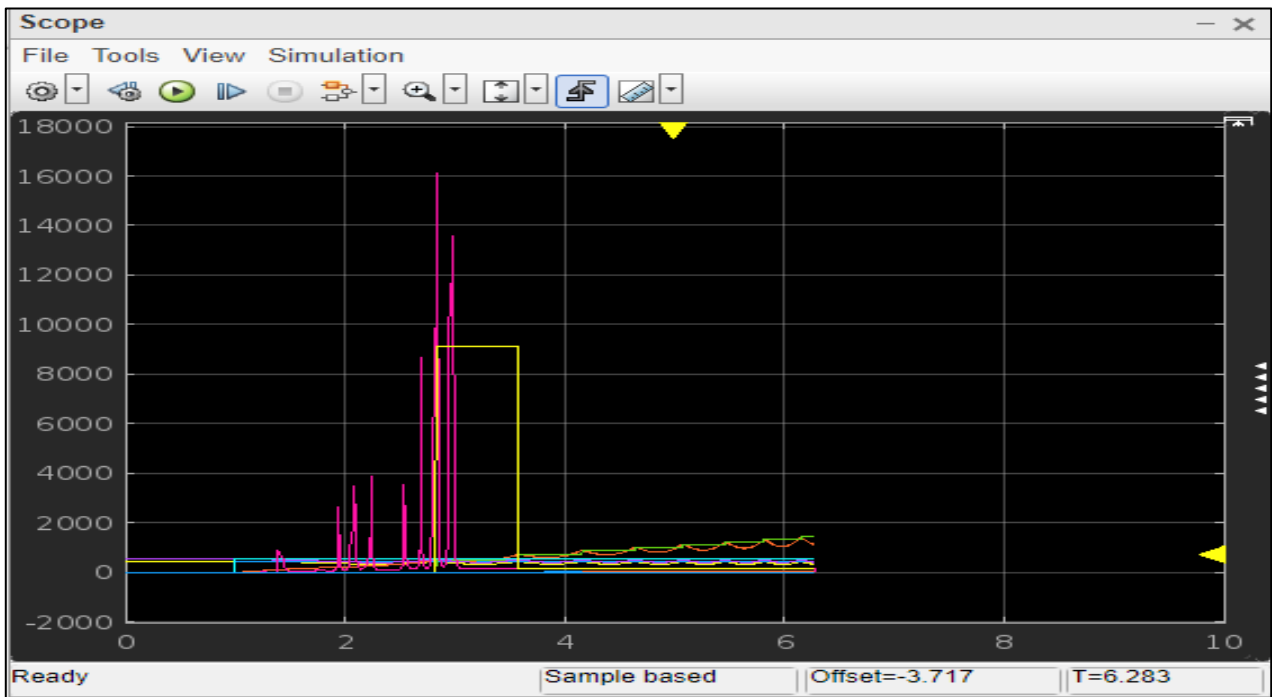


Fig. 13. Harmonic distortion and threshold spectrogram need to be corrected in terms of grammar, technical accuracy, logical coherence, and scientific validity

Harmonic distortion and threshold spectrogram need to be corrected in terms of grammar, technical accuracy, logical coherence, and scientific validity as shown in Figure 14.

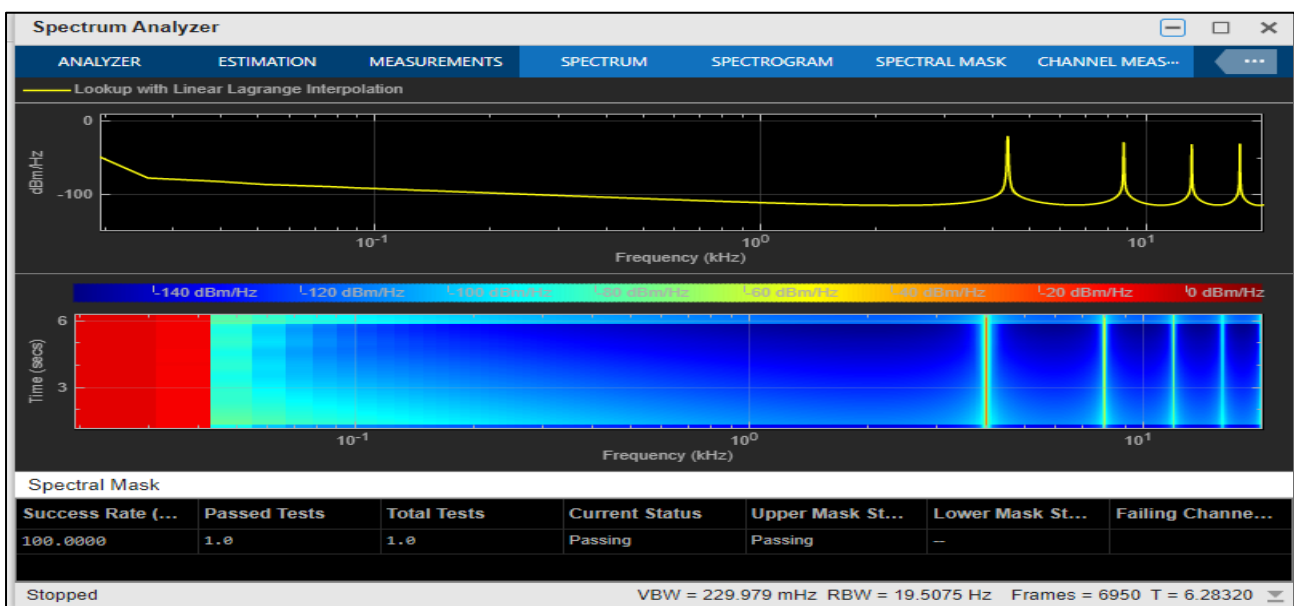


Fig. 14. Frequency versus Time Spectrum Analysis of Sound Using BLDCM for Decibel Distribution

The PMDCM Spectrum Analysis of Frequency vs. Time for sound intensity distribution, as shown in Figure 15, indicates that at the higher density of frequencies towards the end, the noise intensity is observed with higher peaks, and there is a sudden restoration when the frequency returns to the initial state.

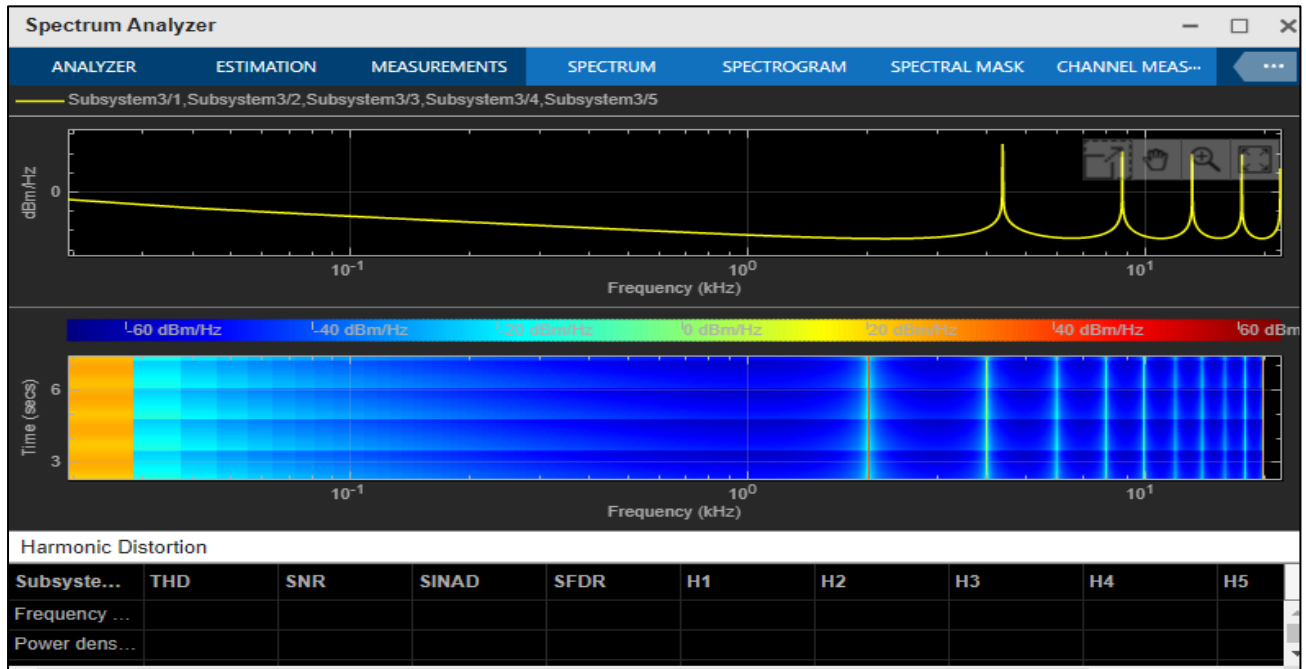


Fig. 15. Frequency versus Time Spectrum Analysis of Sound in Decibel Distribution

The spectrum analysis of a Brushless Direct Current Motor (BLDCM), depicted in Figure 16, reveals intriguing insights into energy distribution over frequency and time domains. Specifically, as illustrated, in regions of higher frequency density, the sound energy spectrum exhibits elevated peaks. These peaks indicate a substantial increase in energy dissipation compared to that of a Permanent Magnet Direct Current Motor (PMDCM).

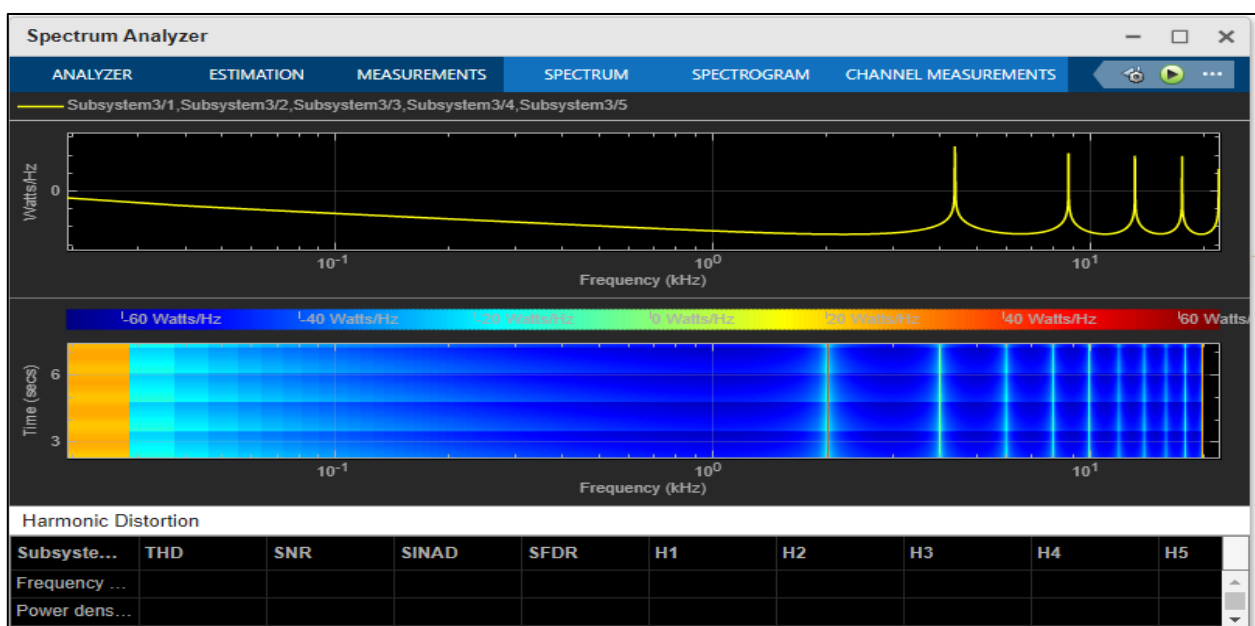


Fig. 16. Frequency and Time Domain Analysis of Sound Energy Distribution in a BLDCM Spectrum

The Spectrum Analysis of PMDCM Frequency vs. Time for Energy Distribution, as depicted in Figure 17, indicates that towards the end, the frequency becomes uniform. This uniformity in frequency is accompanied by a uniformly observed sound energy spectrum. Consequently, the energy dissipation is significantly lower compared to that of a BLDCM.

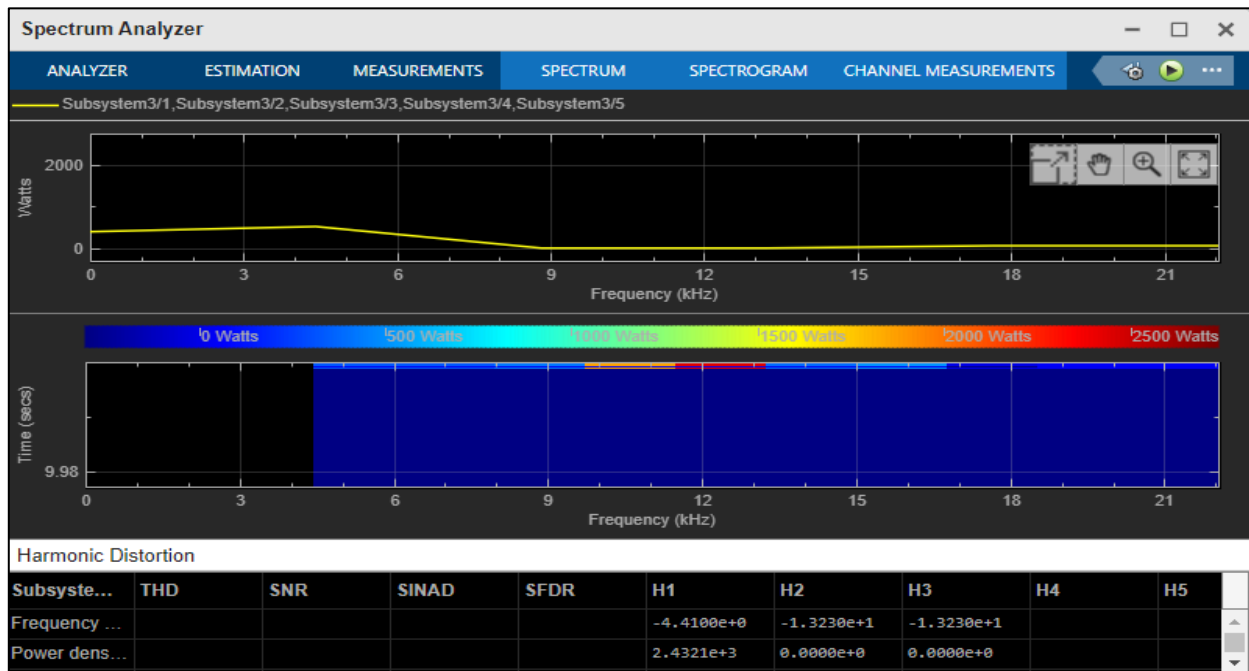


Fig. 17. Spectrum Analysis of PMDCM: Frequency and Time-Based Distribution of Sound Energy

BLDCM Spectrum Analysis: Frequency versus time for energy distribution, as shown in Figure 18, indicates that the overall energy distribution is quite uniform. Therefore, energy dissipation appears to be moderate.

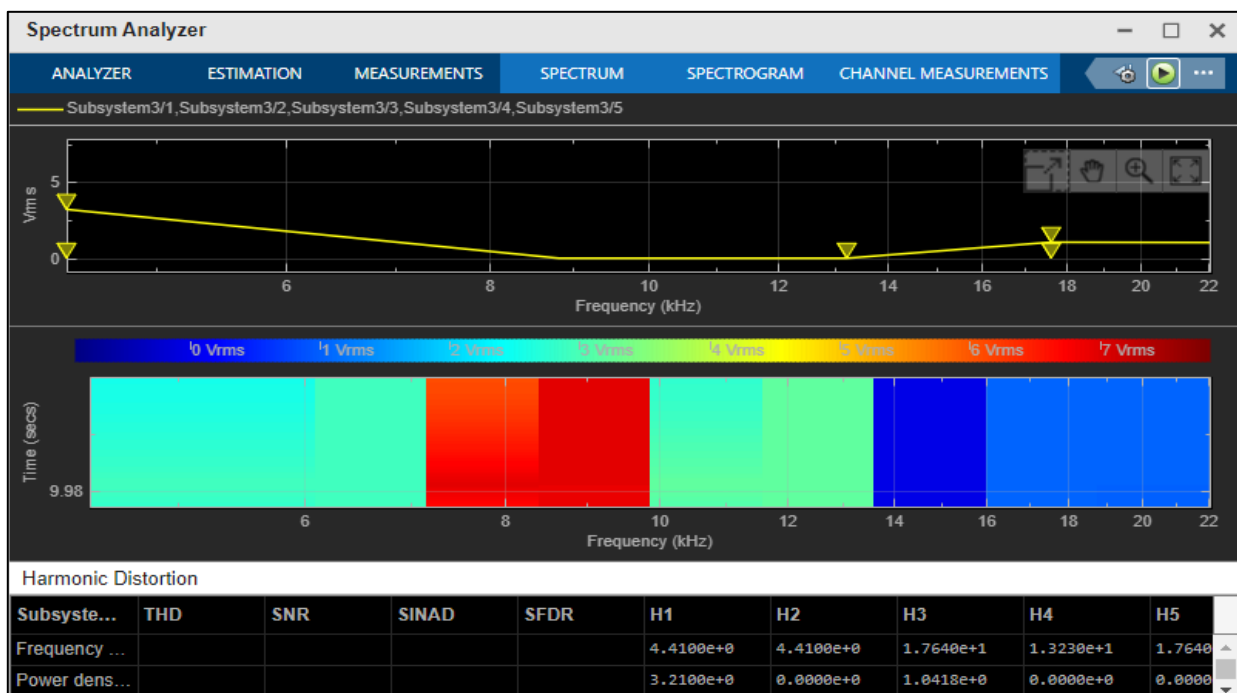


Fig. 18. Analysis of the Spectrum of Frequency versus Time for Overall Energy Distribution in a BLDCM

PMDCM Spectrum Analysis: Frequency versus time for energy distribution, as shown in Figure 19, indicates that the overall energy distribution is varying abruptly. Therefore, uniform energy dissipation is not observed.

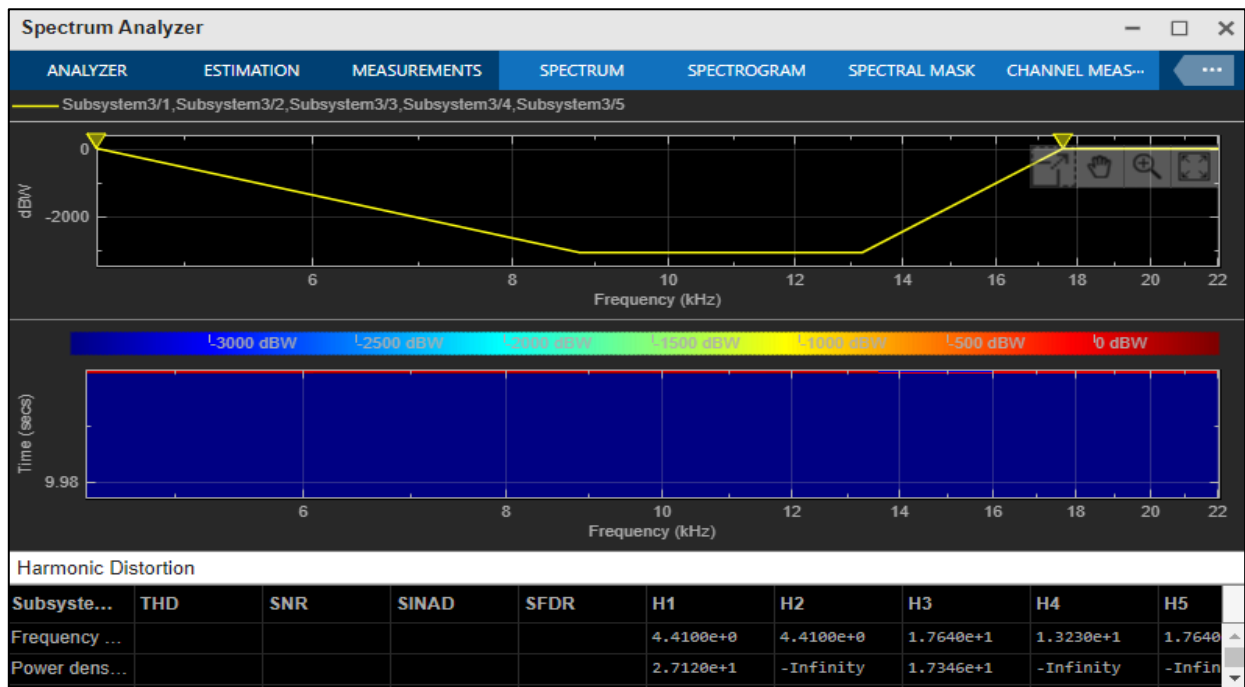


Fig. 19. Perform a PMDCM Spectrum Analysis of Frequency versus Time for the comprehensive distribution of energy

The analysis of the power density spectrum for frequency versus energy distribution of the BLDCM, as shown in Figure 20, indicates that the power density is relatively uniform. Consequently, precise prediction of energy dissipation is feasible.

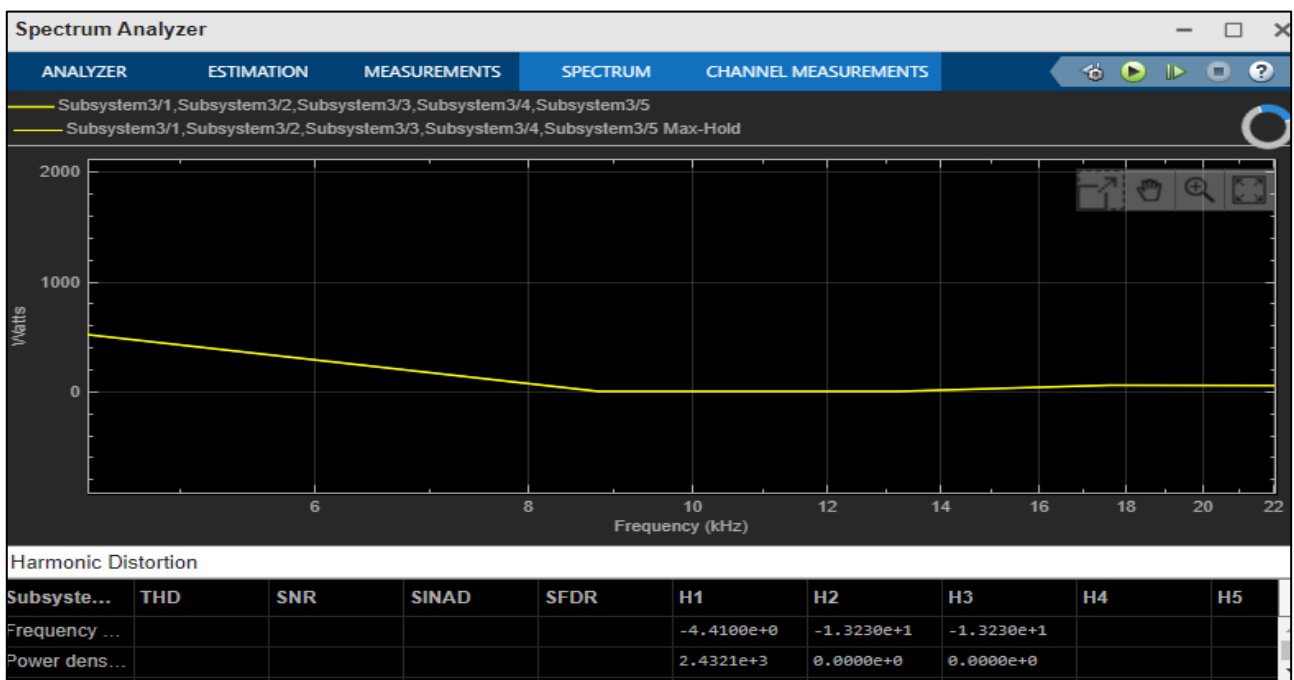


Fig. 20. Power Density Spectrum of BLDCM in the Frequency Domain

The analysis of the power density spectrum for PMDCM in terms of frequency versus energy distribution, as depicted in Figure 21, reveals that power density is not uniformly distributed. Consequently, predicting energy dissipation is not a straightforward task.

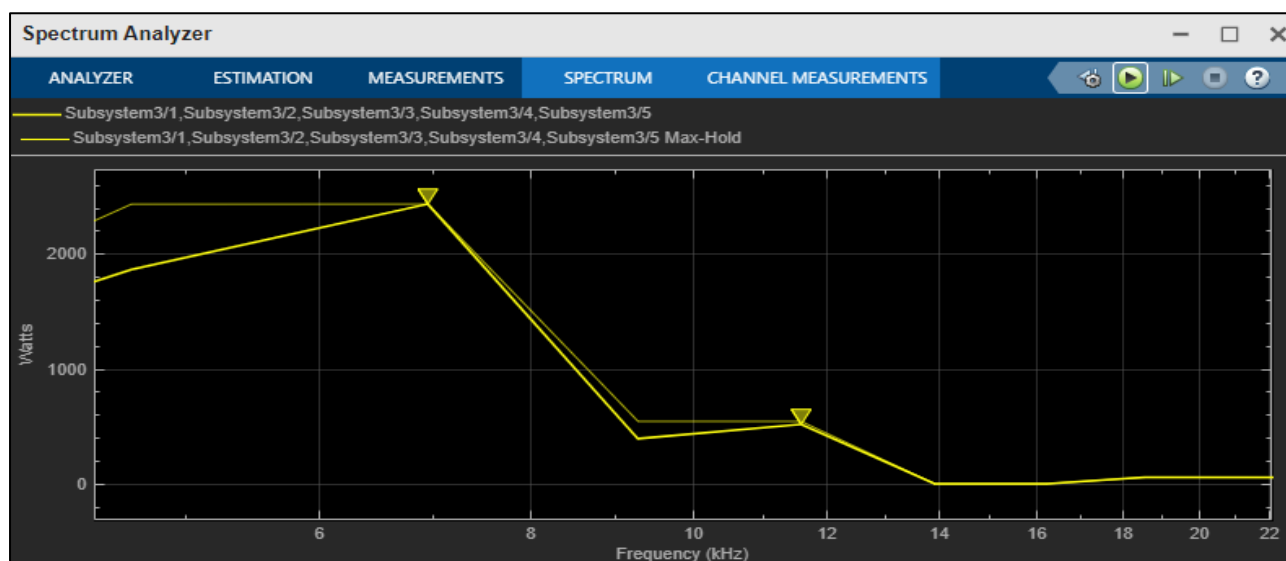


Fig. 21. Power Density Spectrum of PMDCM in the Frequency Domain

3.2.1 Observations

Noisy motors exhibit high Total Harmonic Distortion (THD) levels across various speed steps ranging from 1280 to 7500 RPM. A meaningful one-to-one comparison can only be conducted at the predominant frequency associated with a specific speed. An increase in THD corresponds to a higher level of noise captured by the measuring instrument.

Noisy motors typically manifest lower fundamental components and augmented non-fundamental components. Even harmonic components tend to attenuate as they approach synchronous speed, while odd components persist. Nevertheless, the dissipation of noise-embedded energy can be regulated by closely monitoring motors operating at their resonant frequencies, characterized by shorter wavelengths.

3.2.2 Order of the harmonics

Harmonics refers to voltages or currents occurring at frequencies that are multiples of the fundamental frequency. The universally accepted fundamental frequency is 60 Hz according to global standards. This results in harmonic orders at 120 Hz, 180 Hz, 240 Hz, and so forth. However, for most European countries operating on a 50 Hz frequency system, the harmonic orders become 100 Hz, 150 Hz, 200 Hz, and so on. These orders can be identified by their harmonic numbers or as multiples of the fundamental frequency.

The acoustic noise of the BLDC motor drive is assessed in terms of frequency (Hz), RMS current (A), and Threshold frequency (%r) concerning line or phase voltage. This analysis follows the guidelines set out in ISO 7919-2:2001. The acoustic noise signals surpass the prescribed range outlined in the 85-1980 IEEE Standard, registering at nearly twice the expected levels. The minimum energy required to liberate an electron from a specific metal and the longest wavelength of electromagnetic radiation causing this phenomenon is 235 kJ/mol and is measured in nanometers (nm), respectively.

$$E = hv_o + \frac{1}{2}kV^2 \quad (6)$$

$$\text{Lambdan}, \lambda = \frac{c}{v}, \quad \Phi = v_{th}, \quad v_{th} = \frac{\Phi}{h} \quad (7)$$

$$\Phi = \frac{235 \text{ KJ}}{1 \text{ mole}} \times \frac{1 \text{ mole}}{6.022 \times 10^{23} e^-} \times \frac{1000 \text{ J}}{1 \text{ KJ}}, \quad h = \text{Planks Constant} = 6 \times 10^{34} \text{ J.S} \quad (8)$$

where v_o represents the harmonic stability threshold frequency or electron emission frequency. The variable k is associated with the stiffness-to-mass ratio, while v pertains to the velocity of electrons or the velocity of the machine.

3.3 Waveform Analysis of Line Power Signals' Noise Vectors (Line and Phase Voltages)

The data for BLDCM speed variation in meters per hour against the phase current variation for the noise signal has been simulated. However, the speed fluctuation does not appear to affect the phase current distribution, as illustrated in Figure 22.

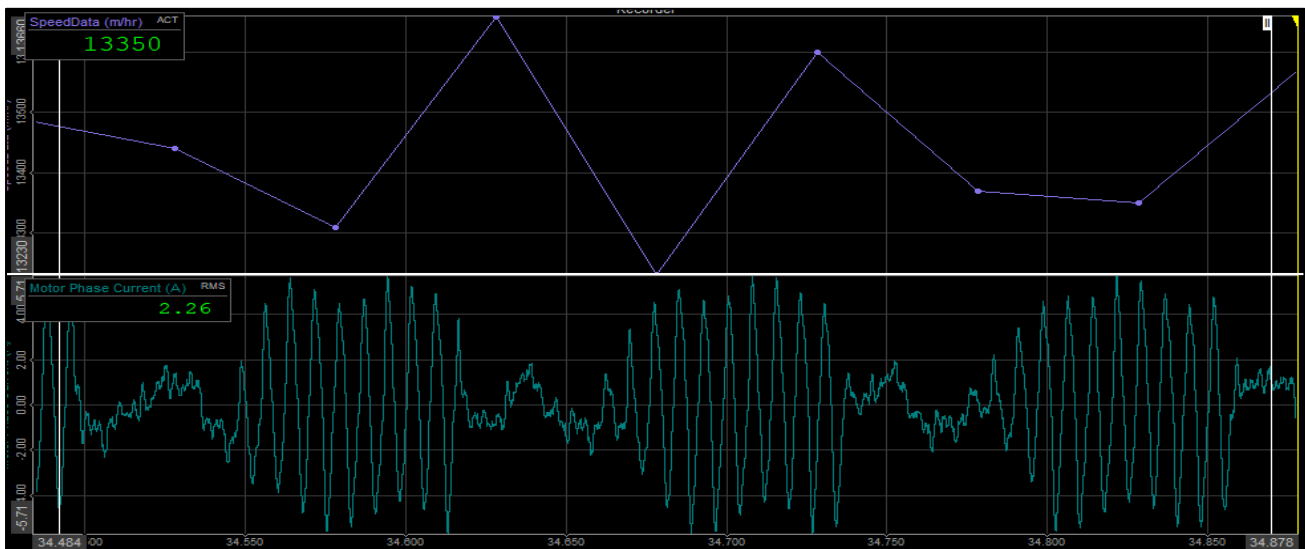


Fig. 22. Performing waveform analysis of the phase current versus speed characteristics of a BLDCM using the DSO-Scientific SM02104X power analyzer

Observations

- No variation in signals was observed in the case of noisy motors and functional (OK)
- The feedback signals of the motors are devoid of high-frequency noise, owing to the frequency limitation of the measurement channel

The speed variation data of PMDCM in meters per hour against the sinusoidal variation of motor phase current is simulated for noise signal analysis. However, the speed remains constant for the sinusoidal distribution of motor phase current, as depicted in Figure 23.

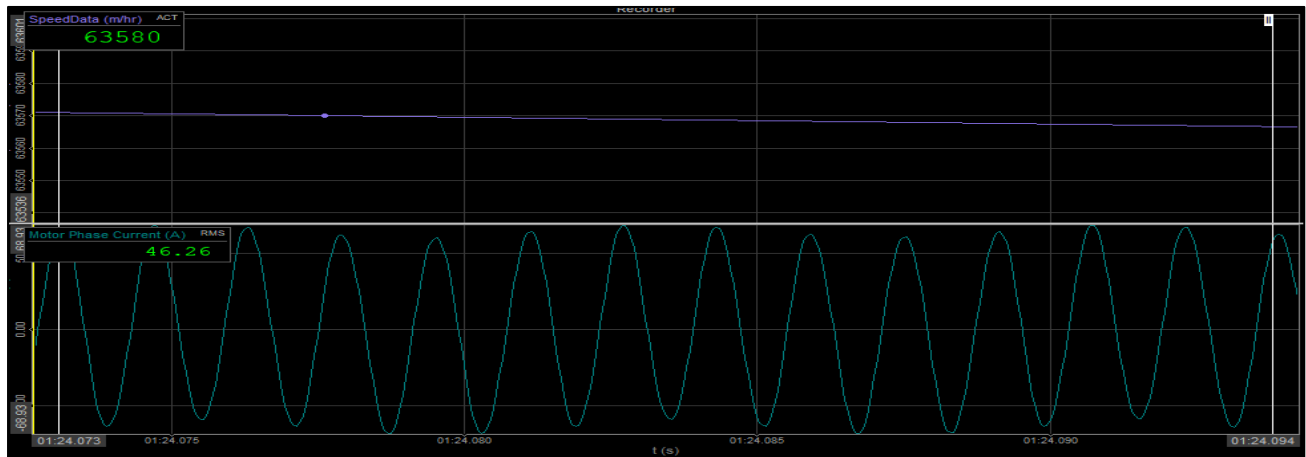


Fig. 23. Waveform analysis of phase current versus speed characteristics of PMDCM (Permanent Magnet DC Motor) using the DSO-Scientific SM02104X Power Analyzer

Observations:

- Distorted sinusoidal current waveform (resulting from current chopping)
- Each phase is conducted for a specific ON time (T_{on}) governed by the MCU (for speed control)
- Harmonic analysis needs to be conducted to capture anomalous noise

As the motor operates at synchronous speed, noisy motors can be identified by analyzing the harmonic contents of the phase current. Other potential sources of noise include electromagnetic factors such as cogging torque and torque ripple, as well as mechanical factors like bearings and rotor vibrations.

4. Results

Noisy motors are identified based on the analysis of phase current harmonic content through waveform analysis of power signals. However, there are additional potential sources of noise induced in the motor due to electromagnetic factors, such as cogging torque, torque ripple, and mechanical aspects like bearings and rotor vibrations. Moreover, the motor's operation can be affected by various field-oriented control (FOC) methods employed by the motor control unit (MCU).

Analyzing the acoustic trends in BLDC/PMDC motor criticality presents challenges for hardware design. To address these challenges, the development of software for modifying control logic using artificial intelligence has become essential to optimize the performance of the BLDC motor. It's important to note that critical considerations arise due to limitations in system and parameter measurements in BLDC motor design.

The insights gained from experimentation and simulation analyses significantly contribute to the advancement of research in areas such as BLDC/PMDC motor dynamics, motor-integrated powertrain, CAN bus communication, and the associated power density analysis.

5. Discussion

The simulation results illustrate that the system's response to a step input is of paramount importance. It governs how effectively the system is designed to achieve its objectives. There exist two primary types of responses: transient response and steady-state response. This simulation experiment employs the BLDC/PMDC motor speed as a step input. This approach serves not only to

identify the system parameters within the control loop but also to optimize its overall performance. The step response reveals the settling time of the operational components within the control loop. Settling time denotes the duration the BLDC motor requires to reach a stable speed in response to the commanded input. Typically, a settling time of 20 seconds is recorded for achieving a steady state.

Initially, the motor produces high torque due to its lower speed. As acceleration commences, the motor departs from the zero-speed range. Once the speed reaches a steady state, the acceleration diminishes to zero again. Within the zero-acceleration zone, precise noise readings can be obtained. This simulation study demonstrates that the resulting speed of the BLDC motor aligns with the desired reference speed, characterized by minimal errors and unfavorable readings in this zone. Before this, it is imperative to ascertain the appropriateness of the selected PI gains.

The step response of the motor concerning current and voltage input showcases the desired energy and power curve. The motor generates power to overcome its inertial resistance and the applied load. To support this imposed load, the motor draws proportionate power from the battery source. In the context of this proposed 4 kW motor, the speed stabilizes into a steady state, and acceleration approaches zero. Nevertheless, the input and output power of the motor theoretically equate.

The energy delivered to the motor is partly utilized to balance power through noise generation, vibration, and subsequent friction-induced heating. The spectrogram depicts the simulation results of energy dissipation with noise frequencies of shorter wavelengths. This study can be further exploited to develop strategies for mitigating the acoustic noise originating from the BLDC/PMDC drive during the design phase.

5.1 Outcome

- i. The noisy motor has a lower fundamental component and higher non-fundamental components.
- ii. Even harmonic frequency components tend to disappear when interfacing with odd components.
- iii. The odd-order harmonics beyond 11 are negligible and should be ignored, as they give rise to dominant frequencies.

6. Conclusion

This paper presents a systematic approach to identifying the noise scale for BLDC motors induced by the internal airspace of both its stator and rotor. The occurrence of acoustic modes as a source of noise in electric motors seems to be quite rare. However, the conventional mechanical and electromagnetic techniques make it challenging to identify the noise sources through the earlier approach focused on the acoustic mode. This paper introduces an experimental study aimed at verifying the influence of acoustic noise under no-load operating conditions of BLDC motors. To evaluate the harmonic stability of the noise analog's 'K' factor, electrical parameters like current frequency, RMS current, and threshold frequency are measured. Subsequently, the motors are classified based on their signal readings for simulation analysis. The simulated analysis undeniably clarifies that electromagnetic forces are the primary cause of acoustic noise in BLDC motors. It has been demonstrated that torque ripple and cogging torque are not responsible for the noise source. However, the acoustic noise signals were found to be almost twice the prescribed range as per the IEEE Standard 85-1980. The contribution of noise scale to overall energy dissipation can be easily

predicted based on this approach. The analysis indicates that approximately 3-4% of the input energy is wasted in this BLDCM/PMDCM setup concerning frequency variation. This is demonstrated in spectrograms showing frequency versus noise amplitude and watts. The predominant frequencies align with where the noise is generated and these frequencies primarily consume the power. This power analysis aids in identifying and segregating noisy motors during assembly.

The scientific power analyzer made by DSO provides power signals along with all associated parameters for analyzing the motors' power characteristics. This analysis helps in identifying energy dissipation due to various factors occurring in such devices. Researchers can leverage this information to design low acoustic noise BLDC motors, especially for more energy-efficient HEV models in customer service.

Acknowledgment

This research is not funded by any agency.

References

- [1] Zhu, Zi-Qiang. "The electromagnetic performance of brushless permanent magnet DC motors-with particular reference to noise and vibration." PhD diss., University of Sheffield, 1991. <https://doi.org/uk.bl.ethos.264816>
- [2] Chen, YangQuan, Ivo Petras, and Dingyu Xue. "Fractional order control tutorial." In *2009 American control conference*, pp. 1397-1411. IEEE, 2009. <https://doi.org/10.1109/ACC.2009.5160719>
- [3] Gamazo-Real, José Carlos, Ernesto Vázquez-Sánchez, and Jaime Gómez-Gil. "Position and speed control of brushless DC motors using sensorless techniques and application trends." *sensors* 10, no. 7 (2010): 6901-6947. <https://doi.org/10.3390/s100706901>
- [4] Bhatnagar, Shalabh Rakesh. "Converting sound energy to electric energy." *International Journal of Emerging Technology and Advanced Engineering* 2, no. 10 (2012): 2250-2459.
- [5] Chattopadhyay, Madhurima, Priyanka Roy, and Sharmi Dutta. "Simulation Modeling of BLDC motor drive and harmonic analysis of stator current, rotor speed, and acceleration using Discrete Wavelet Transform Technique." *Procedia Technology* 4 (2012): 666-670. <https://doi.org/10.1016/j.protcy.2012.05.107>
- [6] Zhang, Dong Ming, Yong Jun Li, and Li Jia Chen. "Simulation of Brushless DC Motor Speed Control Using Phase Locked Loop Based on Noise Analysis." *Advanced Materials Research* 898 (2014): 506-509. <https://doi.org/10.4028/www.scientific.net/AMR.898.506>
- [7] Lee, Hong Joo, Shi Uk Chung, and Sang Moon Hwang. "Noise source identification of a BLDC motor." *Journal of mechanical science and technology* 22 (2008): 708-713. <https://doi.org/10.1007/s12206-008-0110-9>
- [8] Li, Yaohua, Ying Wang, and Xuan Zhao. "Modelling and simulation study on a series-parallel hybrid electric vehicle." *World Electric Vehicle Journal* 7, no. 1 (2015): 133-141. <https://doi.org/10.3390/wevj7010133>
- [9] SENTHILKUMAR, Rajamani, and Venugopal MANIKANDAN. "Design Of Fractional Order PI Controller For DC-DC Boost Converter." *International Journal of Applied Engineering Research* 10, no. 3 (2015): 6883-6900. [https://doi.org/10\(3\):6883-6900](https://doi.org/10(3):6883-6900)
- [10] Qi, Guoyuan. "Energy cycle of brushless DC motor chaotic system." *Applied Mathematical Modelling* 51 (2017): 686-697. <https://doi.org/10.1016/j.apm.2017.07.025>
- [11] Xia, Kun, Zhengrong Li, Jing Lu, Bin Dong, and Chao Bi. "Acoustic noise of brushless DC motors induced by electromagnetic torque ripple." *Journal of Power Electronics* 17, no. 4 (2017): 963-971. <https://doi.org/10.6113/JPE.2017.17.4.963>
- [12] Dr. S. K. Mahobia, "STUDY AND ANALYSIS OF PERMANENT MAGNET DC MOTORS WITH VARIOUS PARAMETERS", *International Journals of Research Granthaalayah*, ISSN- 2350-0530(O), ISSN- 2394-3629(P), 2017. <https://doi.org/10.5281/zenodo.345632>
- [13] Pindoriya, R. M., A. K. Mishra, B. S. Rajpurohit, and R. Kumar. "An analysis of vibration and acoustic noise of BLDC motor drive." In *2018 IEEE Power & Energy Society General Meeting (PESGM)*, pp. 1-5. IEEE, 2018. <https://doi.org/10.1109/PESGM.2018.8585750>
- [14] Kumar, A. Sathish, K. Sami, and A. Ananthi Christy. "Speed Control of Brushless DC Motor." *Indian Journal of Public Health Research & Development* 9, no. 10 (2018). <https://doi.org/10.5958/0976-5506.2018.01238.X>
- [15] SARANKAR, DURGESH, and ASHISH KUMAR SINGHAL. "Mathematical Modeling of DC-DC Converter." *Iconic Research And Engineering Journals* 1, no. 9 (2018). <https://doi.org/10.1155/2018/2536946>

- [16] Djekidel, Rabah, Ahmed Sid Bessedik, and Abdechafik Hadjadj. "Electric field modeling and analysis of EHV power line using improved calculation method." *Facta Universitatis-series: Electronics and Energetics* 31, no. 3 (2018): 425-445. <https://doi.org/10.2298/FUEE1803425D>
- [17] Prajapati, Saurav, Man Mohan Garg, and Boddu Prithvi. "Design of fractional-order PI controller for DC-DC power converters." In *2018 8th IEEE India International Conference on Power Electronics (IICPE)*, pp. 1-6. IEEE, 2018. <https://doi.org/10.1109/IICPE.2018.8709430>
- [18] Lee, Jongkyong, Kibum Jung, and Sungjun Park. "Simulation of radiated emissions from a low voltage bldc motor." In *2018 International Symposium on Antennas and Propagation (ISAP)*, pp. 1-2. IEEE, 2018.
- [19] Barod, Yogesh Singh, and Alka Thakur. "Mathematical Modelling and Analysis of BLDC Motor for Vibration and Noise Effect Along with Current Variation." *International Journal of Research in Engineering, Science and Management* 2, no. 11. <https://doi.org/10.1109/PESGM.2018.8585750>
- [20] Hoyos, Fredy E., John E. Candelo-Becerra, and Carlos I. Hoyos Velasco. "Model-based quasi-sliding mode control with loss estimation applied to DC-DC power converters." *Electronics* 8, no. 10 (2019): 1086. <https://doi.org/10.3390/electronics8101086>
- [21] Wang, Yongchao, Hui Gao, Haiyang Wang, and Wenpeng Ma. "NVH optimization analysis of permanent magnet synchronous motor by rotor slotting." *Vehicles* 2, no. 2 (2020): 287-302. <https://doi.org/10.3390/vehicles2020016>
- [22] Gupta, Ishita, and Akash Varshney. "Speed-Torque Characteristics of BLDC Motor with Load Variations." (2020).
- [23] Soriano-Sánchez, Allan G., Martín A. Rodríguez-Licea, Francisco J. Pérez-Pinal, and José A. Vázquez-López. "Fractional-order approximation and synthesis of a PID controller for a buck converter." *Energies* 13, no. 3 (2020): 629. <https://doi.org/10.3390/en13030629>
- [24] Bogdan, Virlan, Munteanu Adrian, Livadaru Leonard, Bobu Alexandra, Simion Alecsandru, and Nacu Ionut. "Design and optimization of a BLDC motor for small power vehicles." In *2021 International Conference on Electromechanical and Energy Systems (SIEMEN)*, pp. 438-443. IEEE, 2021. <https://doi.org/10.1109/SIEMEN53755.2021.9600327>
- [25] Fu, Zhaoyang, Xingbang Liu, and Jinglin Liu. "Research on the fault diagnosis of dual-redundancy BLDC motor." *Energy Reports* 7 (2021): 17-22. <https://doi.org/10.1016/j.egy.2021.02.032>
- [26] Chaithanya, D. J., S. Anitha, B. Ramya, and A. P. Aisiri. "Power Generation Using Sound by Piezo Electric Material." In *Journal of Physics: Conference Series*, vol. 1916, no. 1, p. 012003. IOP Publishing, 2021. <https://doi.org/10.1088/1742-6596/1916/1/012003>
- [27] Mervin A. Boco, "Sound energy harvesting and converting electricity (SEHCE)", *Annals of Mathematics and Physics*, ISSN 2689-7636, (4 October 2022). <https://doi.org/10.17352/amp.000056>
- [28] Maybury, Lucy, Pdraig Corcoran, and Liana Cipcigan. "Mathematical modelling of electric vehicle adoption: A systematic literature review." *Transportation Research Part D: Transport and Environment* 107 (2022): 103278. <https://doi.org/10.1016/j.trd.2022.103278>
- [29] Pathan, Khizar Ahmed, Prakash S. Dabeer, and Sher Afghan Khan. "Investigation of base pressure variations in internal and external suddenly expanded flows using CFD analysis." *CFD Letters* 11, no. 4 (2019): 32-40.
- [30] Pathan Khizar Ahmed, Syed Ashfaq, Prakash S Dabeer, and Sher Afgan Khan. "Analysis of parameters affecting thrust and base pressure in suddenly expanded flow from nozzle." *Journal of Advanced Research in Fluid Mechanics and Thermal Sciences* 64, no. 1 (2019): 1-18.
- [31] Pathan, Khizar Ahmed, Prakash S. Dabeer, and Sher Afghan Khan. "Influence of expansion level on base pressure and reattachment length." *CFD Letters* 11, no. 5 (2019): 22-36.
- [32] Khan, Ambareen, Nurul Musfirah Mazlan, and Ervin Sulaeman. "Effect of Ribs as Passive Control on Base Pressure at Sonic Mach Numbers." *CFD Letters* 14, no. 1 (2022): 140-151. <https://doi.org/10.37934/cfdl.14.1.140151>
- [33] Shamitha, Asha Crasta, Khizar Ahmed Pathan, and Sher Afghan Khan. "Numerical simulation of surface pressure of a wedge at supersonic Mach numbers and application of design of experiments." *Journal of advanced research in applied mechanics* 101: 1-18. <https://doi.org/10.37934/aram.101.1.118>
- [34] Shamitha, Crasta Asha, Khizar Ahmed Pathan, and Sher Afghan Khan. "Analytical and Numerical Simulation of Surface Pressure of an Oscillating Wedge at Hypersonic Mach Numbers and Application of Taguchi's Method." *Journal of Advanced Research in Applied Sciences and Engineering Technology* 30, no. 1 (2023): 15-30. <https://doi.org/10.37934/araset.30.1.1530>
- [35] Shaikh, Sohel Khalil, Khizar Ahmed Pathan, Zakir Ilahi Chaudhary, B. G. Marlpalle, and Sher Afghan Khan. "An Investigation of Three-Way Catalytic Converter for Various Inlet Cone Angles Using CFD." *CFD Letters* 12, no. 9 (2020): 76-90. <https://doi.org/10.37934/cfdl.12.9.7690>
- [36] Shaikh, Sohel Khalil, Khizar Ahmed Pathan, Zakir Ilahi Chaudhary, and Sher Afghan Khan. "CFD analysis of an automobile catalytic converter to obtain flow uniformity and to minimize pressure drop across the monolith." *CFD Letters* 12, no. 9 (2020): 116-128. <https://doi.org/10.37934/cfdl.12.9.116128>